Journal of The Electrochemical Society, 2024 **171** 100525
1945-7111/2024/171(10)/100525/7/$40.00 © 2024 The Electrochemical Society ("ECS"). Published on behalf of ECS by IOP Publishing Limited.

Exploring the Optimal Binder Content in Composite Electrodes for Sulfide-Based All-Solid-State Lithium-Ion Batteries

Yong-Han Jo,[1] Young-Jun Lee,[2] and Dong-Won Kim[1,2,z]

[1]*Department of Battery Engineering, Hanyang University, Seoul 04763, Republic of Korea*
[2]*Department of Chemical Engineering, Hanyang University, Seoul 04763, Republic of Korea*

All-solid-state batteries (ASSBs) are promising next-generation batteries owing to their improved safety compared with lithium-ion batteries using flammable liquid electrolytes. Among various solid electrolytes, sulfide-based electrolytes exhibit high ionic conductivities, and their ductile properties allow them to be easily processed without high-temperature sintering. In sulfide-based ASSBs, a polymer binder is essential for achieving a good cycling performance by maintaining strong interfacial contacts in the composite electrodes during cycling. In this study, we prepared a composite Si-C anode and a $LiNi_{0.82}Co_{0.1}Mn_{0.08}O_2$ cathode using a nitrile-butadiene rubber binder for ASSB applications, and investigated the effect of the binder content on the mechanical properties and electrochemical performance. The binder content significantly influenced the physical and electrochemical characteristics of the composite electrodes, and the ASSB prepared with 1.5 wt% binder showed the best cycling performance considering capacity retention and rate capability. Furthermore, we investigated how the excess binder adversely affected the cycling performance through time-of-flight secondary ion mass spectrometry analysis.
 [DOI: 10.1149/1945-7111/ad851f]

Manuscript submitted July 31, 2024; revised manuscript received October 2, 2024. Published October 18, 2024.

Supplementary material for this article is available online

The use of fossil fuels, such as coal and petroleum, has increased the emission of greenhouse gases, such as carbon dioxide, resulting in global warming. Hence, eco-friendly electric vehicles that can reduce carbon emissions have attracted attention worldwide.[1–3] However, the lithium-ion batteries (LIBs) employed in electric vehicles currently use flammable liquid electrolytes, which cause thermal runaway and explosion under abnormal conditions. Therefore, all-solid-state batteries (ASSBs) that use solid electrolytes have been actively investigated as next-generation batteries to enhance battery safety.[4–6]

Among the various solid electrolyte systems, sulfide electrolytes, such as $25Li_2S\text{-}75P_2S_5$, Li_6PS_5X (X: Cl, Br, I) and $Li_{10}GeP_2S_{12}$, exhibit high ionic conductivities, and their ductility allows them to be easily processed without high-temperature sintering.[5,7–9] However, several technical challenges remain in the commercialization of ASSBs. Unlike in LIBs, composite electrodes containing solid electrolytes should be employed when assembling ASSBs. The composite electrodes composed of active material, solid electrolyte, conducting carbon, and binder undergo large volume changes during repeated cycling, which weaken the interfacial contact among the electrode components and thus disconnect the transport pathways of electrons and Li^+ ions in the composite electrodes.[10,11] Therefore, the use of an appropriate polymer binder that maintains interfacial contact by providing strong adhesion is important for achieving good cycling performance in ASSBs.[12–16] Nitrile butadiene rubber (NBR) is commonly used as a wet process binder in the composite electrodes for ASSBs, because it exhibits high adhesive properties and good solubility in less polar or nonpolar solvents.[17–20] Our research group has reported that the composite cathode using NBR25 (nitrile content: 25 wt%) revealed the best performance with respect to mechanical and electrochemical properties.[20] Nitrile groups that induce ion–dipole interactions with other electrode components lead to strong adhesion, contributing to the maintenance of good interfacial contact.[21–23]

In this study, we explored the optimal binder content in a composite $LiNi_{0.82}Co_{0.10}Mn_{0.08}O_2$ (NCM) cathode and a Si-graphite (Si-C) anode. The composite cathodes and anodes were prepared with different NBR binder contents (0.5–2.5 wt%), and the effect of binder content on the mechanical properties and cycling performance was investigated. Our results revealed that the polymer binder content played a pivotal role in achieving stable cycling and good high-rate performance in sulfide-based all-solid-state LIBs.

Experimental

Materials.—Ball-milled graphite flakes (Fritsch), Si (Hanbyul), and sucrose (Sigma Aldrich) with a mass ratio of 55:35:10 were used to synthesize Si-graphite granules. The mixture was dispersed in deionized water and spray-dried through the spray dryer (Eyela) at a rotating speed of 500 rpm and 110 °C. The obtained Si-graphite granule was heated at 90 °C and coated with coal-tar pitch (TCK) at 500 rpm for 30 min by an attrition-type mill.[24] Polycrystalline $LiNi_{0.82}Co_{0.10}Mn_{0.08}O_2$ (NCM) supplied by L & F Co., Ltd has been coated by boron-based oxide. Super C carbon was purchased from Timcal Co. Ltd. Si-graphite, NCM, and Super C were dried in a vacuum oven at 110 °C for 12 h. Li_6PS_5Cl (LPSCl, argyrodite) of different particle sizes was supplied by Jeong Kwan Co., Ltd. The larger size ($d_{50} = 3\ \mu m$) was used for preparing a solid electrolyte pellet, and the smaller size ($d_{50} = 1\ \mu m$) was used in fabricating the composite electrodes. NBR with 25 wt% nitrile was provided by Kumho Petrochemical Co., Ltd. N-butyl butyrate was purchased from Alfa Aesar. Lithium (200 μm) and indium metals (100 μm) were supplied by Honjo Metal Co., Ltd and Nilaco, respectively.

Preparation of the composite electrode.—NBR was dissolved in n-butyl butyrate to produce a 5 wt% binder solution. The composite NCM cathode was obtained by casting the homogeneous slurry consisting of NCM, LPSCl, Super C, and NBR with a mass ratio of 70:28.5:1.5:x ($0.5 \leqslant x \leqslant 2.5$) on an Al current collector. The composite anode was also fabricated from the mixture of Si-C, LPSCl, and NBR (70:30:x by mass ratio, $0.5 \leqslant x \leqslant 2.5$) on a Ni current collector. All the composite electrodes were vacuum-dried at 90 °C for 6 h to remove residual solvent. The thickness of the composite NCM cathode was 100 μm and that of the composite Si-C anode was 30 μm. The active mass loadings in the composite cathode and anode were approximately 11.0 and 2.5 mg cm^{-2}, respectively.

Cell assembly.—The solid electrolyte was fabricated by compressing LPSCl powder at 300 MPa. The obtained composite electrode (composite NCM cathode or composite Si-C anode) was placed on the solid electrolyte pellet and pressed at 420 MPa. The Li–In was then placed opposite to the composite electrode. Finally, the assembled half-cell was subjected to a torque of 11 Nm, which

[z]E-mail: dongwonkim@hanyang.ac.kr

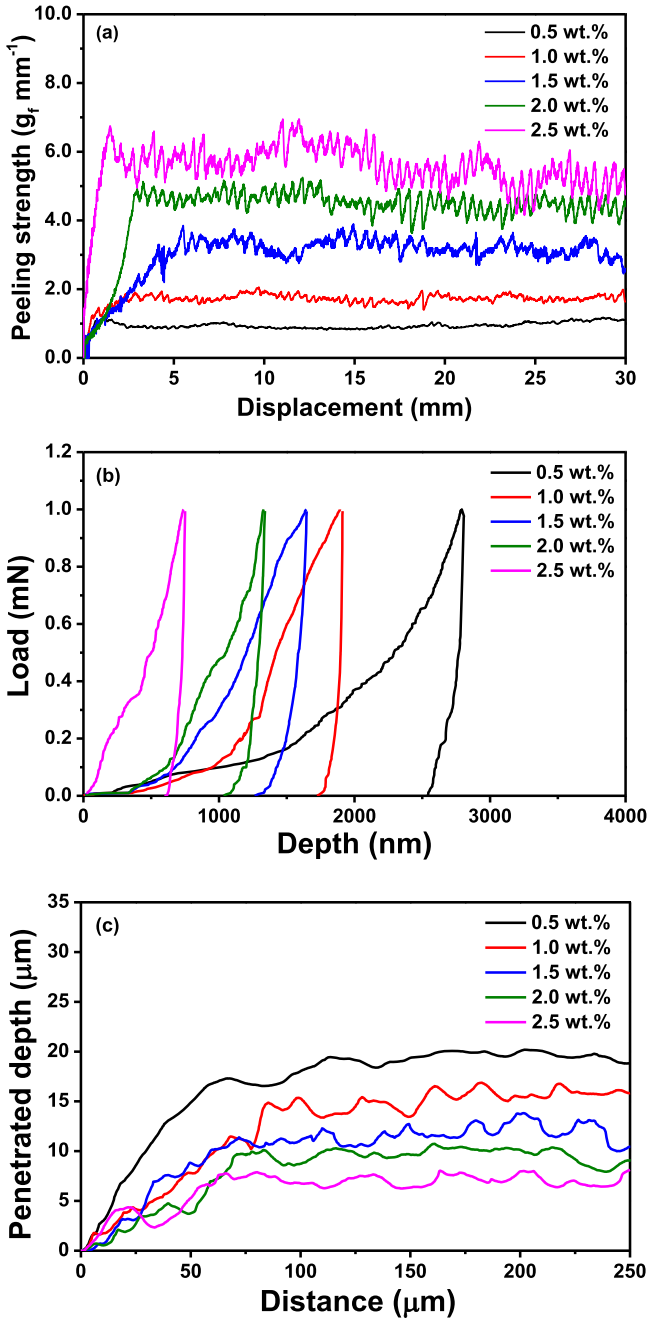

Figure 1. (a) Peeling strength of the composite cathodes with different binder contents. (b) Nanoindentation load–depth curves and (c) nanoscratch curves of the composite cathodes.

corresponded to a stack pressure of 75 MPa. The lithium-ion full-cell was also assembled by sandwiching a solid electrolyte pellet between the composite Si-C anode and the composite NCM cathode, followed by pressing at 420 MPa. All the procedures for cell assembly were conducted in a high-purity argon atmosphere glove box (MBRAUN, moisture < 0.1, $O_2 < 0.1$ ppm).

Characterization and measurements.—The adhesion test of the composite electrode was conducted using a universal testing machine (QM100SE, QMESYS). Nanoindentation and nanoscratch analyses were performed using the NanoTest Vantage platform. A pressure sensor (GS-I-210, GS Co., Ltd) was placed in the pressurized cell to conduct operando electrochemical pressiometry measurements. Time-of-flight secondary ion mass spectrometry (TOF-SIMS) was conducted using a TOF SIMS 5 (ION-TOF GmbH) to investigate the remaining Li^+ ions in the composite Si-C anode with an imaging area of $50 \times 50\ \mu m^2$. The assembled cell was subjected to preconditioning at 0.05 C before the cycling test, where 1.0 C corresponds to 2.0 mA cm^{-2} for the composite NCM cathode and 2.8 mA cm^{-2} for the composite Si-C anode. The galvanostatic cycling of the half-cells and full-cells was conducted at 0.5 C with battery cycling equipment (WBCS 3000, WonATech) at 30 °C. The ionic and electronic conductivities of the composite electrodes were measured with a symmetric SUS/composite electrode/SUS cell using an impedance analyzer (ZIVE MP1, WonATech). The galvanostatic intermittent titration technique (GITT) measurements were conducted to obtain the relative active surface area of the NCM. The cell was subjected to repeated discharge pulses of 0.1 C for 60 s and allowed to rest for 60 min. For direct current internal resistance (DC-IR) measurements, the cell was subjected to cycling at 0.05 C rate. Subsequently, after charging to 3.1 V, it underwent charge and discharge pulses of increasing C rates (0.025 to 1.0 C) for 10 s, followed by rest for 20 min.

Results and Discussion

To confirm the structural stability of LPSCl toward n-butyl butyrate and NBR during slurry casting process, the XRD pattern of LPSCl/NBR(70.0/1.5 by mass) composite was compared to that of pristine LPSCl. As shown in Fig. S1a, the XRD pattern of LPSCl was not changed in the LPSCl/NBR composite that was prepared by slurry casting using n-butyl butyrate, indicating that LPSCl is chemically stable with n-butyl butyrate and NBR. In addition, the XRD pattern of composite cathode in Fig. S1b revealed that all the crystalline peaks of LPSCl and NCM maintained well in the

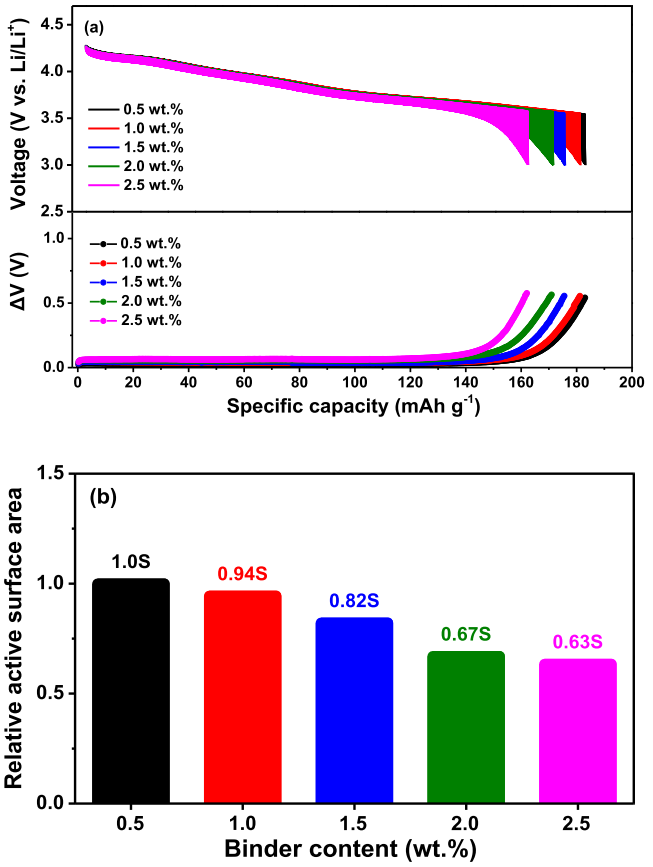

Figure 2. (a) Voltage curves of the composite cathodes with different binder contents during GITT experiments. (b) Relative active surface area between NCM and LPSCl in the composite cathodes.

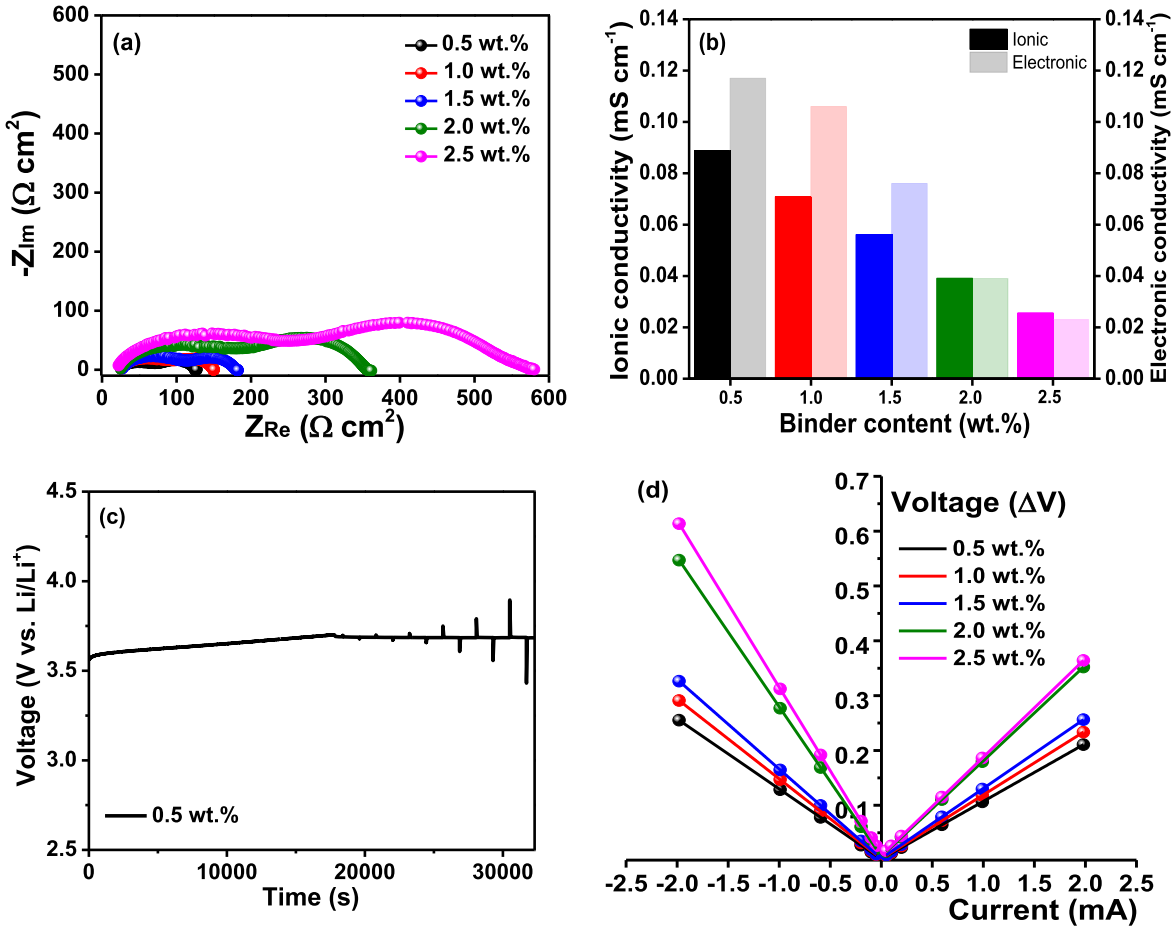

Figure 3. (a) Electrochemical impedance spectra of the symmetrical SUS/composite cathode/SUS cells. (b) Ionic and electronic conductivities of the composite cathodes. (c) Voltage response of the Li-In/NCM cell with 0.5 wt% NBR during DC-IR experiments. (d) Plots of the change in voltage vs current of the cells employing the composite cathodes with different binder contents.

composite cathode, which implies no interfacial side reactions between NCM and LPSCl.

A peeling test at 180° was conducted to compare the adhesion strength of the composite cathodes. For the peeling test, the composite cathode attached to the $20 \times 30\ mm^2$ tape was pulled at a speed of $30\ mm\ min^{-1}$. As shown in Fig. 1a, the peeling strength increased with increasing binder content. Thus, the composite cathode with 2.5 wt% NBR exhibited the highest peeling strength. These results reveal that an increase in the binder content contributes to the enhancement of the adhesive strength between the current collector and cathode components.[25] Nanoindentation experiments were conducted to investigate the mechanical properties of the composite cathodes. A sharp indenter was used to measure the penetration depth of the composite cathode (Fig. 1b). As the binder content increased, the penetration depth gradually decreased, which can be interpreted as an improvement in the cohesive properties of the composite cathode. The penetration depth vs scraped distance curves for the nanoscratch experiment are presented in Fig. 1c. The higher the binder content in the composite cathode, the lower the penetrated depth, indicating the superior cohesion properties in the composite cathode with high binder contents.[26] These results demonstrate that a high polymer binder content enhances the mechanical properties of the composite cathode in terms of adhesive and cohesive strength.

GITT analysis was conducted to study the effect of binder content on the electrochemical properties of the composite cathode. The voltage profiles obtained during the GITT experiments are shown in Fig. 2a. As shown in the figure, the cathode with 0.5 wt% NBR exhibited the highest discharge capacity and the lowest overpotential. From the GITT data, the relative active surface area of the active material in the composite cathode was estimated using the following equation,[15]

$$D = \frac{4}{\pi\tau}\left(\frac{n_m V_m}{S}\right)^2\left(\frac{\Delta E_s}{\Delta E_t}\right)^2$$

where D is the diffusion coefficient of Li^+ ions in NCM, τ is the pulse duration time, n_m and V_m are the number of moles and molar volume of NCM, respectively, S is the active surface area of NCM, ΔE_s is the steady-state voltage change, and ΔE_t is the transient voltage change. When the composite cathodes are in the same charge state, they have similar diffusion coefficients.[27–29] Accordingly, the relative active surface area (S) is influenced by the voltage changes, ΔE_s and ΔE_t, depicted in Fig. S2. When the active surface area of NCM in the composite cathode with 0.5 wt% binder was set to 1.0S, the relative active surface areas of the NCM active material in the other composite cathodes were 0.94S, 0.82S, 0.67S, and 0.63S, as presented in Fig. 2b. These results indicate that the addition of polymer binder to the composite NCM cathode reduces the active surface area between cathode active material and solid electrolyte.

A lithium-ion-blocking symmetrical cell (SUS/composite cathode/SUS) was fabricated to understand the effect of reducing the active surface area on the electrical conduction properties of the composite NCM cathode.[30,31] The carbon additive was excluded from the composite cathode because the electronic conductivity should be maintained at low levels.[32] AC impedance spectra of cells with different binder contents are shown in Fig. 3a. The resulting ionic and electronic conductivities of the composite NCM cathodes,

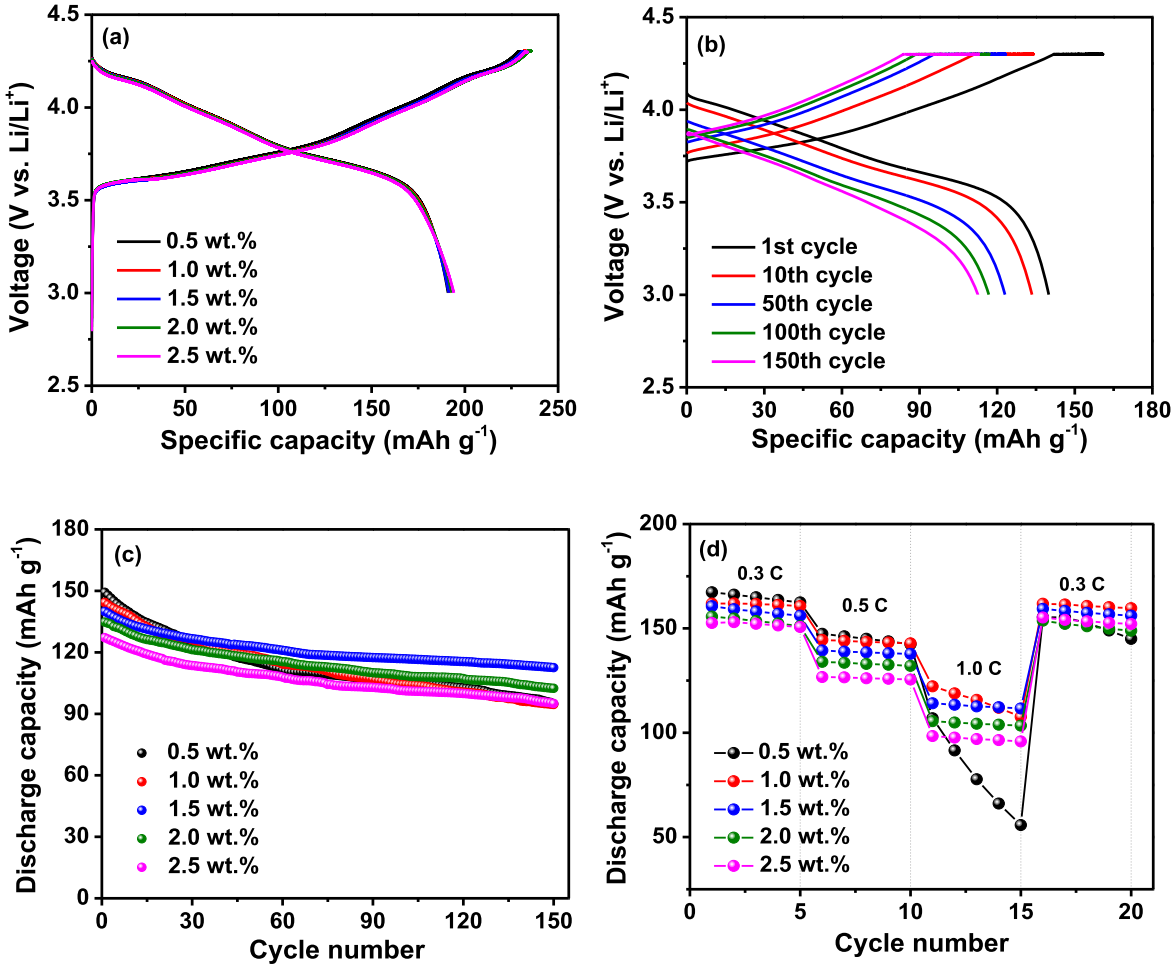

Figure 4. (a) Voltage profiles of the cells employing composite cathodes with different binder contents during the preconditioning cycle at 0.05 C rate. (b) Charge and discharge curves of the cell prepared with 1.5 wt% NBR at 0.5 C and (c) discharge capacities of the cells employing composite cathodes with different binder contents at 0.5 C. (d) Discharge capacities of the cells as a function of the current rate.

calculated using the transmission line model, are shown in Fig. 3b. As expected, the ionic and electronic conductivities gradually decreased with increasing binder content. These results are consistent with the DC polarization measurements shown in Fig. S3. The voltage responses of the Li-In/NCM half-cells at different current densities during the DC-IR experiments are shown in Figs. 3c and S4. The internal resistance of the composite NCM cathode was determined from the linear slope of the change in voltage vs current (Fig. 3d).[33,34] The slopes during discharge are larger than those during charge, because the intercalation of lithium ions into active materials is kinetically sluggish compared to their deintercalation, as previously reported.[15,33] The composite NCM cathode with higher binder content exhibited a higher slope, indicating a high resistance owing to the disturbance in the transport of Li^+ ions and electrons. From these results, it is understood that, although increasing the binder content reinforces the mechanical properties of the composite cathode, it causes an increase in the internal resistance with a reduction in the ionic and electronic conductivities owing to the decrease in the active surface area and disturbance of the Li^+ ion and electron conduction pathways.

Cycling performance of the composite NCM cathodes with different binder contents was investigated, and the results are shown in Fig. 4. The voltage curves of the Li-In/NCM half-cells during the first preconditioning cycle at 30 °C and 0.05 C are depicted in Fig. 4a. At the preconditioning cycle, the cells showed almost the same overpotential and discharge capacities ranging from 191.0 to 194.1 mAh g^{-1}. Figure 4b shows the charge–discharge curves of the composite cathode with 1.5 wt% binder at a rate of 0.5 C, and the cycling performance of the composite cathodes with different binder contents was compared in Fig. 4c. After constant current charging at 0.5 C rate, the constant voltage charge was applied, because it improved the capacity and cycling stability at high current rate. The initial discharge capacity of the cells decreased with increasing binder content owing to an increase in cell resistance. With respect to the cycling stability, the composite cathodes with 0.5 and 1.0 wt% binder exhibited large capacity fading owing to inferior adhesive and cohesive properties. Among the investigated electrodes, the composite cathode with 1.5 wt% binder showed the highest capacity retention after 150 cycles. The cross-sectional SEM images of the composite NCM cathodes before and after cycles are presented in Fig. S5. Before cycling, the composite NCM cathodes exhibited good interfacial adhesion between electrode components. However, they showed the loss of interfacial contacts after 150 cycles due to the volumetric changes of NCM during cycling. To compare the void space caused by the loss of interfacial contacts between cathode components, we obtained black and white images using the ImageJ software, as depicted in Fig. S6. The composite NCM cathodes before cycling had almost same porosities of about 3.0%. After cycling, the porosities were increased to 15.0, 11.2, and 9.0% in the composite NCM cathodes with 0.5, 1.5 and 2.5 wt% binder, respectively. These results indicate that the interfacial adhesion is enhanced with increasing binder content, although the electrical resistances in the composite NCM cathode increases, as previously discussed. Figure 4d presents the discharge capacities of the composite cathodes as a function of C rate. Despite the low resistance of the composite cathode with 0.5 wt% binder, it exhibited

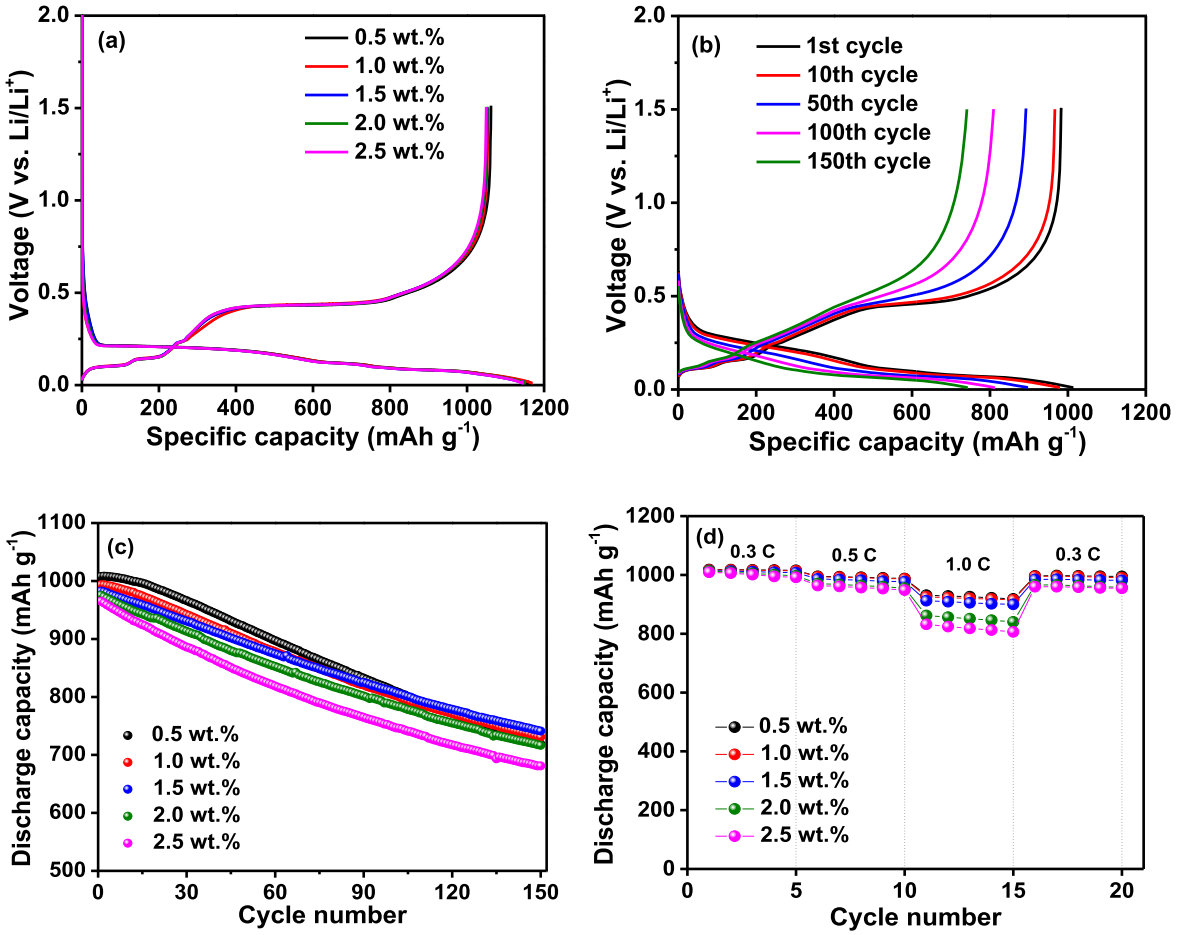

Figure 5. (a) Voltage profiles of the cells employing composite Si-C anodes with different binder contents during the preconditioning cycle at 0.05 C rate. (b) Charge and discharge curves of the Li-In/Si-C cell prepared with 1.5 wt% NBR at 0.5 C and (c) discharge capacities of the cells employing composite Si-C anodes with different binder contents at 0.5 C. (d) Discharge capacities of the cells as a function of the current rate.

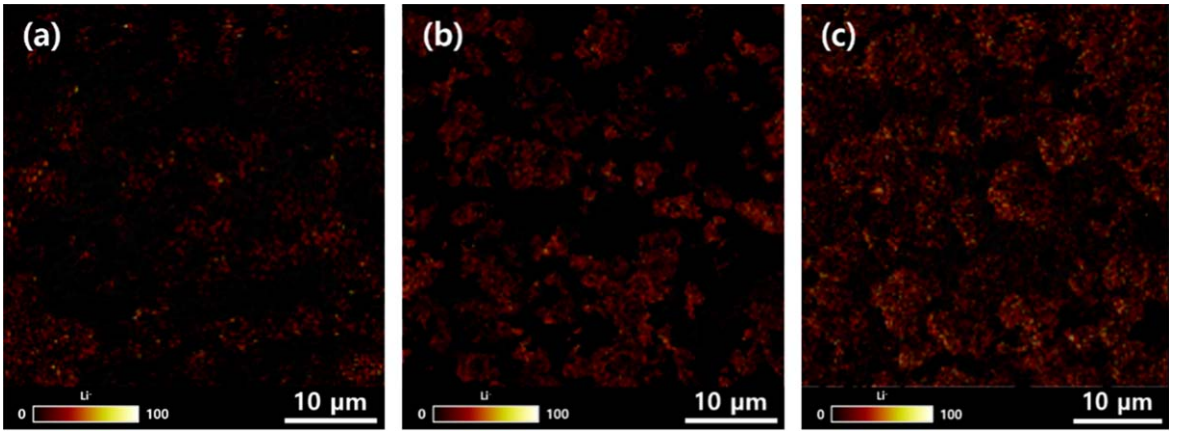

Figure 6. TOF-SIMS image mappings in the negative Li-ion mode of the surface of the composite Si-C anodes with different binder contents at the delithiated state after 15 cycles at 0.5 C. (a) 0.5 wt%, (b) 1.5 wt%, and (c) 2.5 wt%.

low capacities and large capacity fading at 1.0 C cycling, which can be attributed to the poor interfacial adhesion between electrode components (active material, solid electrolyte, and conducting carbon). The composite cathode with 1.5 wt% binder showed the best cycling performance with respect to high-rate capability and cycling stability. These results indicate that the optimal binder content for balancing strong adhesive properties and low internal resistance is approximately 1.5 wt% in the composite NCM cathode for ASSBs.

Figure S7 shows the voltage profiles and corresponding pressure changes of the Li-In/NCM half-cells with different binder contents during 0.5 C cycling. During the charging process, the cell pressure was increased because of the volume expansion of the Li-In anode. In contrast, the cell pressure was decreased when the Li^+ ions moved from the Li-In anode to the composite cathode during the discharge cycle. As shown in Fig. S7f, the Li-In/NCM half-cell with 0.5 wt% binder experienced the highest pressure change before and after 10 cycles. This result suggests that some residual Li^+ ions

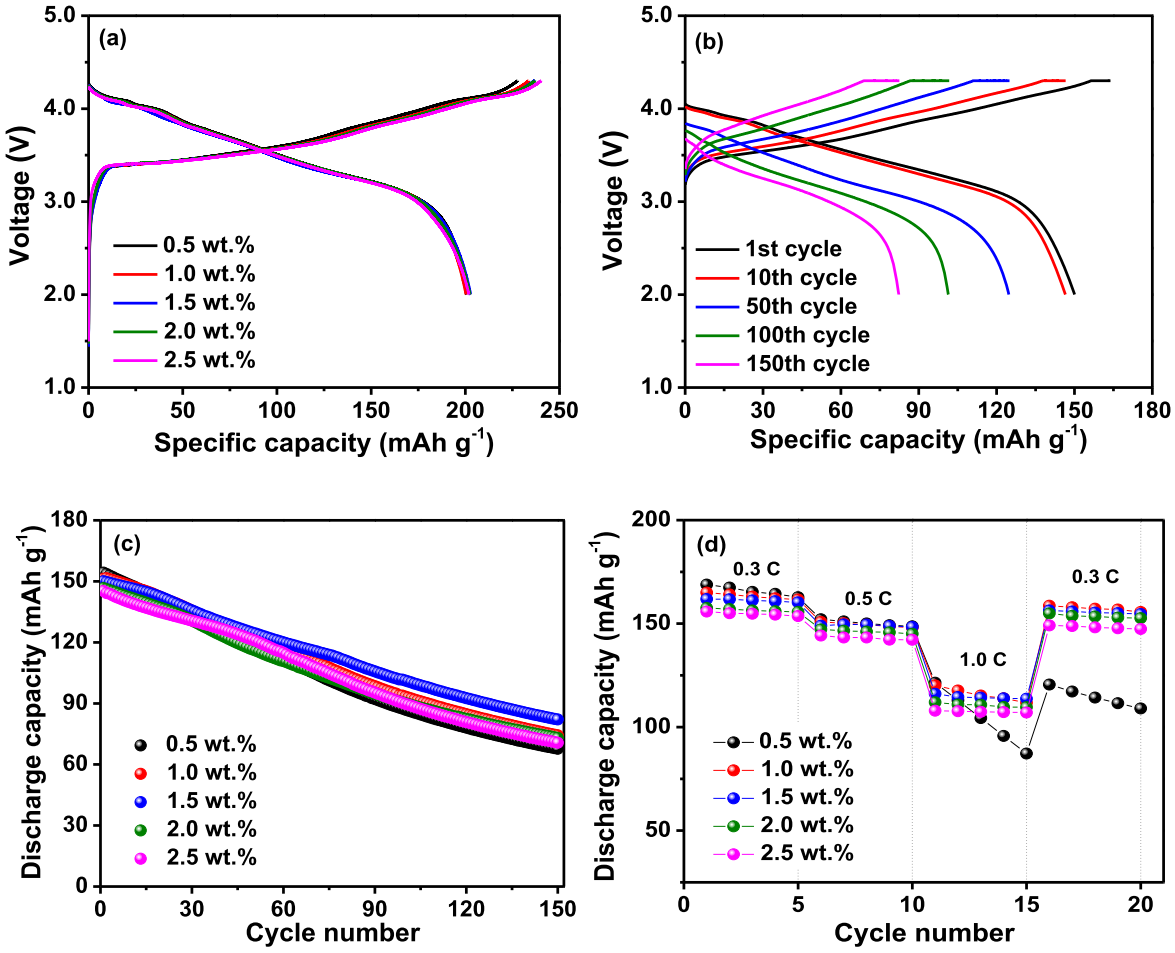

Figure 7. (a) Voltage profiles of the all-solid-state Si-C/NCM cells during the preconditioning cycle at 0.05 C rate. (b) Voltage curves of the cells with 1.5 wt% binder at 0.5 C. (c) Discharge capacities of the cells at 0.5 C. (d) Discharge capacities of the cells with different current rates.

remain on the anode side after cycling, resulting in a large change in cell pressure.

Composite Si-C anodes were assembled using the same NBR binder, and their mechanical property was evaluated. As shown in Fig. S8, the peeling strength of the composite anode was increased with binder content. The electronic and ionic conductivities of composite Si-C anodes are presented in Fig. S9. It is noticeable that the electronic conductivities are quite high due to the presence of conductive carbon in the composite Si-C anodes. As expected, both electronic and ionic conductivities of composite Si-C anodes were decreased with the content of binder. The composite Si-C anodes exhibited lower ionic conductivities than those of composite NCM cathodes, since Si has lower Li^+ diffusion coefficient than NCM material.

The electrochemical performance of composite Si-C anodes are presented in Fig. 5. As shown in Fig. 5a, the composite Si-C anodes delivered high discharge capacities in the range of 1,050 to 1,062 mAh g^{-1} based on the active Si-C material during the first preconditioning cycle at 0.05 C. Figure 5b shows the voltage profiles of the Li-In/Si-C half-cell with 1.5 wt% NBR at 0.5 C rate, and the cycling performance of the cells employing different binder contents is compared in Fig. 5c. When the binder content was low (0.5 wt%), the cell exhibited a high initial discharge capacity but large capacity fading after 60 cycles owing to its insufficient binding properties, which cannot accommodate the volume change of Si-C in the composite anode. Excess binder (2.5 wt%) resulted in a low initial discharge capacity and poor capacity retention, and the cell employing 1.5 wt% binder showed the best cycling stability owing to the balanced properties of interfacial adhesion and cell resistance.

Figure 5d shows the discharge capacities of the composite Si-C anodes at different current rates. In contrast to the composite NCM cathode, the composite anode with 0.5 wt% binder exhibited the highest discharge capacity and good capacity retention at a rate of 1.0 C. TOF-SIMS analysis was conducted to investigate why the composite Si-C anode with 0.5 wt% binder exhibited the best cycling performance at 1.0 C despite its inadequate binding properties. The Li^- maps of the composite Si-C anode in the fully delithiated state after 15 cycles are shown in Fig. 6. The Li^- signals originating from the Li-Si and Li_xC_6 phases increased with increasing binder content.[35–37] These results indicate that the composite Si-C anode with a low binder content was effective for Li^+ ion extraction from the active materials during the de-lithiation process, resulting in a superior cycling performance under high current conditions.

Finally, all-solid-state lithium-ion full cells were assembled by sandwiching a solid electrolyte pellet between the composite Si-C anode and the composite NCM cathode, and their cycling performance was investigated. Figure 7a shows the voltage profiles of the cells within the cutoff voltages between 2.0 and 4.3 V at the preconditioning cycle. The cells initially delivered similar discharge capacities based on the cathode active material. Figure 7b shows the charge and discharge curves of the all-solid-state full-cell employing 1.5 wt% binder at 0.5 C and 30 °C. The cycling stability and rate capability of the cells with different binder contents are compared in Figs. 7c and 7d, respectively. The capacity fading of the cells with different amounts of NBR is mainly related with the increase of interfacial resistances in the composite electrodes due to the deterioration of adhesive and cohesive properties with the repeated

cycling. The cell with 0.5 wt% binder showed a high initial discharge capacity but a large capacity decline owing to the inferior interfacial adhesion within the composite electrode. By contrast, the cell employing 2.5 wt% binder exhibited a poor capacity retention despite its strong adhesion properties. This is because the charge-transfer reaction was retarded in the composite Si-C anode with a high binder content, as previously discussed. Overall, the all-solid-state lithium-ion cell with a composite Si-C anode and NCM cathode employing 1.5 wt% binder showed the best cycling performance with respect to capacity retention and rate capability. These results reveal that 1.5 wt% of NBR binder is optimal for ensuring good binding properties and maintaining low internal resistance, which resulted in a good cycling performance of ASSBs.

Conclusions

In this study, we explored the optimal binder content in composite Si-C anodes and composite NCM cathodes for ASSBs by evaluating their mechanical properties and electrochemical performance. An increase in binder content enhanced the binding properties of the composite electrodes in terms of adhesion and cohesion. However, the cell resistance increased due to the reduction in the active surface area of the active materials, resulting in the interruption of the Li^+ ion and electron pathways. Moreover, an excessive amount of binder induced residual lithium ions in the composite anode after de-lithiation. The cycling test and rate capability results revealed that low binder content made it difficult to maintain sufficient binding within the composite electrodes. Accordingly, the use of 1.5 wt% NBR binder demonstrated the best cycling performance in the ASSB composed of the composite Si-C anode, Li_6PS_5Cl solid electrolyte, and composite NCM cathode.

Acknowledgments

This study was supported by the Technology Innovation Program (20024827), funded by the Ministry of Trade, Industry, and Energy (MOTIE, Korea).

ORCID

Young-Jun Lee https://orcid.org/0000-0003-0956-4454
Dong-Won Kim https://orcid.org/0000-0002-1735-0272

References

1. F. Wu, J. Maier, and Y. Yu, "Guidelines and trends for next-generation rechargeable lithium and lithium-ion batteries." *Chem. Soc. Rev.*, **49**, 1569 (2020).
2. N. Rietmann, B. Hugler, and T. Lieven, "Forecasting the trajectory of electric vehicle sales and the consequences for worldwide CO_2 emissions." *J. Clean. Prod.*, **261**, 121038 (2020).
3. Z. Yang, H. Huang, and F. Lin, "Sustainable electric vehicle batteries for a sustainable world: perspectives on battery cathodes, environment, supply Chain, manufacturing, life cycle, and policy." *Adv. Energy Mater.*, **12**, 2200383 (2022).
4. J. Liang, J. Luo, Q. Sun, X. Yang, R. Li, and X. Sun, "Recent progress on solid-state hybrid electrolytes for solid-state lithium batteries." *Energy Storage Mater.*, **21**, 308 (2019).
5. Y. Kato, S. Hori, T. Saito, K. Suzuki, M. Hirayama, A. Mitsui, M. Yonemura, H. Iba, and R. Kanno, "High-power all-solid-state batteries using sulfide superionic conductors." *Nat. Energy*, **1**, 16030 (2016).
6. Z. Gao, H. Sun, L. Fu, F. Ye, Y. Zhang, W. Luo, and Y. Huang, "Promises, challenges, and recent progress of inorganic solid-state electrolytes for all-solid-state lithium batteries." *Adv. Mater.*, **30**, 1705702 (2018).
7. N. Kamaya et al., "A lithium superionic conductor." *Nat. Mater.*, **10**, 682 (2011).
8. Y. Seino, T. Ota, K. Takada, A. Hayashi, and M. Tatsumisago, "A sulphide lithium super ion conductor is superior to liquid ion conductors for use in rechargeable batteries." *Energy Environ. Sci.*, **7**, 627 (2014).
9. A. Banerjee, X. Wang, C. Fang, E. A. Wu, and Y. S. Meng, "Interfaces and interphases in all-solid-state batteries with inorganic solid electrolytes." *Chem. Rev.*, **120**, 6878 (2020).
10. W. Zhang et al., "Interfacial processes and influence of composite cathode microstructure controlling the performance of all-solid-state lithium batteries." *ACS Appl. Mater. Interfaces*, **9**, 17835 (2017).
11. R. Koerver, W. Zhang, L. de Biasi, S. Schweidler, A. O. Kondrakov, S. Kolling, T. Brezesinski, P. Hartmann, W. G. Zeier, and J. Janek, "Chemo-mechanical expansion of lithium electrode materials—on the route to mechanically optimized all-solid-state batteries." *Energy Environ. Sci.*, **11**, 2142 (2018).
12. K. Lee, S. Kim, J. Park, S. H. Park, A. Coskun, D. S. Jung, W. Cho, and J. W. Choi, "Selection of binder and solvent for solution-processed all-solid-state battery." *J. Electrochem. Soc.*, **164**, A2075 (2017).
13. Y. J. Nam, D. Y. Oh, S. H. Jung, and Y. S. Jung, "Toward practical all-solid-state lithium-ion batteries with high energy density and safety: comparative study for electrodes fabricated by dry- and slurry-mixing processes." *J. Power Sources*, **375**, 93 (2018).
14. D. Y. Oh, Y. J. Nam, K. H. Park, S. H. Jung, K. T. Kim, A. R. Ha, and Y. S. Jung, "Slurry-fabricable Li^+-conductive polymeric binders for practical all-solid-state lithium-ion batteries enabled by solvate ionic liquids." *Adv. Energy Mater.*, **9**, 1802927 (2019).
15. S.-B. Hong, Y.-J. Lee, U.-H. Kim, C. Bak, Y. M. Lee, W. Cho, H. J. Hah, Y.-K. Sun, and D.-W. Kim, "All-solid-state lithium batteries: Li^+ -conducting ionomer binder for dry-processed composite cathodes." *ACS Energy Lett.*, **7**, 1092 (2022).
16. S.-B. Hong, Y.-R. Jang, H. Kim, Y.-C. Jung, G. Shin, H. J. Hah, W. Cho, Y.-K. Sun, and D.-W. Kim, "Wet-processable binder in composite cathode for high energy density all-solid-state lithium batteries." *Adv. Energy Mater.*, **14**, 2400802 (2024).
17. K. Kim, J. Park, G. Jeong, J.-S. Yu, Y.-C. Kim, M.-S. Park, W. Cho, and R. Kanno, "Rational design of a composite electrode to realize a high-performance all-solid-state battery." *ChemSusChem*, **12**, 2637 (2019).
18. J. Lee, K. Lee, T. Lee, H. Kim, K. Kim, W. Cho, A. Coskun, K. Char, and J. W. Choi, "In situ deprotection of polymeric binders for solution-processible sulfide-based all-solid-state batteries." *Adv. Mater.*, **32**, 2001702 (2020).
19. K. T. Kim, D. Y. Oh, S. Jun, Y. B. Song, T. Y. Kwon, Y. Han, and Y. S. Jung, "Tailoring slurries using cosolvents and Li salt targeting practical all-solid-state batteries employing sulfide solid electrolytes." *Adv. Energy Mater.*, **11**, 2003766 (2021).
20. Y.-J. Lee, S.-B. Hong, and D.-W. Kim, "Exploring the use of butadiene rubbers as a binder in composite cathodes for all-solid-state lithium batteries." *J. Ind. Eng. Chem.*, **122**, 341 (2023).
21. L. Gong, M. H.-T. Nguyen, and E.-S. Oh, "High polar polyacrylonitrile as a potential binder for negative electrodes in lithium ion batteries." *Electrochem. Commun.*, **29**, 45 (2013).
22. L. Luo, Y. Xu, H. Zhang, X. Han, H. Dong, X. Xu, C. Chen, Y. Zhang, and J. Lin, "Comprehensive understanding of high polar polyacrylonitrile as an effective binder for Li-ion battery nano-Si anodes." *ACS Appl. Mater. Interfaces*, **8**, 8154 (2016).
23. G. Yoo, S. Kim, C. Chanthad, M. Cho, and Y. Lee, "Elastic rubber-containing multifunctional binder for advanced Li-S batteries." *Chem. Eng. J.*, **405**, 126628 (2021).
24. D. Lee, A. Kondo, S. Lee, S. Myeong, S. Sun, I. Hwang, T. Song, M. Naito, and U. Paik, "Controlled swelling behavior and stable cycling of silicon/graphite granular composite for high energy density in lithium ion batteries." *J. Power Sources*, **457**, 228021 (2020).
25. J. Hu, Y. Wang, D. Li, and Y.-T. Cheng, "Effects of adhesion and cohesion on the electrochemical performance and durability of silicon composite electrodes." *J. Power Sources*, **397**, 223 (2018).
26. S. N.-S. Hapuarachchi, K. C. Wasalathilake, J. Y. Nerkar, E. Jaatinen, A. P. O'Mullane, and C. Yan, "Mechanically robust tapioca starch composite binder with improved ionic conductivity for sustainable lithium-ion batteries." *ACS Sustain. Chem. Eng.*, **8**, 9857 (2020).
27. X. Yang and A. L. Rogach, "Electrochemical techniques in battery research: a tutorial for nonelectrochemists." *Adv. Energy Mater.*, **9**, 1900747 (2019).
28. K. H. Park, D. Y. Oh, Y. E. Choi, Y. J. Nam, L. Han, J.-Y. Kim, H. Xin, F. Lin, S. M. Oh, and Y. S. Jung, "Solution-processable glass LiI-Li_4SnS_4 superionic conductors for all-solid-state Li-ion batteries." *Adv. Mater.*, **28**, 1874 (2016).
29. J. Kim, S. Park, S. Hwang, and W.-S. Yoon, "Principles and applications of galvanostatic intermittent titration technique for lithium-ion batteries." *J. Electrochem. Sci. Technol.*, **13**, 19 (2022).
30. A. S. Keefe, S. Buteau, I. G. Hill, and J. R. Dahn, "Temperature dependent EIS studies separating charge transfer impedance from contact impedance in lithium-ion symmetric cells." *J. Electrochem. Soc.*, **166**, A3272 (2019).
31. H. Nara, D. Mukoyama, T. Yokoshima, T. Momma, and T. Osaka, "Impedance analysis with transmission line model for reaction distribution in a pouch type lithium-ion battery by using micro reference electrode." *J. Electrochem. Soc.*, **163**, A434 (2016).
32. Z. Siroma, T. Sato, T. Takeuchi, R. Nagai, A. Ota, and T. Ioroi, "AC impedance analysis of ionic and electronic conductivities in electrode mixture layers for an all-solid-state lithium-ion battery." *J. Power Sources*, **316**, 215 (2016).
33. D. Zhang, B. S. Haran, A. Durairajan, R. E. White, Y. Podrazhansky, and B. N. Popov, "Studies on capacity fade of lithium-ion batteries." *J. Power Sources*, **91**, 122 (2000).
34. Y. Shimonishi, D. Mori, Y. Maeda, S. Taminato, N. Imanishi, and S. Yoshida, "Investigation of the difference in charge/discharge resistance for cathode materials after cycle test combined with STEM-EELS and XAFS analysis." *J. Electrochem. Soc.*, **168**, 040533 (2021).
35. Y. Feng, B. M. Koo, A. Seyeux, J. Swiatowska, C. Henry de Villeneuve, M. Rosso, and F. Ozanam, "ToF-SIMS Li depth profiling of pure and methylated amorphous silicon electrodes after their partial lithiation." *ACS Appl. Mater. Interfaces*, **14**, 35716 (2022).
36. Z.-Y. Wu, Y.-Q. Lu, J.-T. Li, S. Zanna, A. Seyeux, L. Huang, S.-G. Sun, P. Marcus, and J. Swiatowska, "Influence of carbonate solvents on solid electrolyte interphase composition over Si electrodes monitored by in situ and ex situ spectroscopies." *ACS Omega*, **6**, 27335 (2021).
37. F. Walther, R. Koerver, T. Fuchs, S. Ohno, J. Sann, M. Rohnke, W. G. Zeier, and J. Janek, "Visualization of the interfacial decomposition of composite cathodes in argyrodite-based all-solid-state batteries using time-of-flight secondary-ion mass spectrometry." *Chem. Mater.*, **31**, 3745 (2019).